NANO LETTERS

LETTER

pubs.acs.org/NanoLett

Growth of Straight Silicon Nanowires on Amorphous Substrates with Uniform Diameter, Length, Orientation, and Location Using Nanopatterned Host-Mediated Catalyst

Chao Wang,[†] Patrick F. Murphy,[†] Nan Yao,[‡] Kevin McIlwrath,[§] and Stephen Y. Chou*[,†]

[†]Nanostructure Laboratory, Department of Electrical Engineering, and [‡]PRISM Imaging and Analysis Center, Princeton University
[§]Hitachi High Technologies America, Inc.

ABSTRACT: We report a new approach, termed "growth by nanopatterned host-medicated catalyst" (NHC growth), to solve nonuniformities of Si nanowires (NWs) grown on amorphous substrates. Rather than pure metal catalyst, the NHC uses a mixture of metal catalyst with the material to be grown (i.e., Si), nanopatterns them into desired locations and anneals them. The Si host ensures one catalyst-dot per-growth-site, prevents catalyst-dot break-up, and crystallizes catalyst-dot (hence orientating NWs). The growth results straight silicon NWs on SiO_2 with uniform length and diameter (4% deviation), predetermined locations, preferred orientation, one-wire per-growth-site, and high density; all are 10−100 times better than conventional growth.

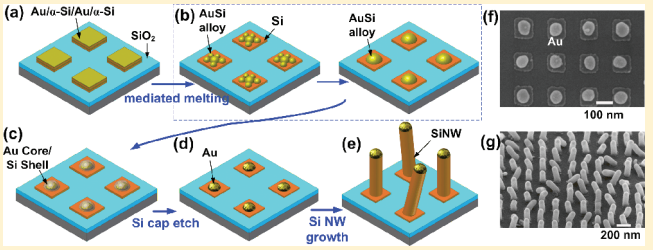

KEYWORDS: Si nanowire, amorphous substrate, growth, guided growth, nanopatterned catalyst, host mediation, nanoimprint lithography

Semiconductor nanowires (NWs) offer a broad range of potential significant applications from integrated circuits,[1,2] lasers,[3] solar cells[4] to displays[5] and biosensors,[6] to name just a few.[7] The epitaxial growth on a crystalline substrate (e.g., a (111) Si) using vapor−liquid−solid (VLS) method[8] and localized metal catalyst nanostructures (e.g., Au nanodots) can result in straight single-crystal Si NWs of uniform length, diameter and wire-orientation, as well as one wire per single catalyst dot.[9−11] Despite enormous efforts, however, a central challenge has been that the NWs grown on amorphous substrates do not have such properties. The growth on an amorphous substrate with the same nanodot catalyst and growth conditions results in (a) curved and twist NWs having large variations in NW's length, diameter, and wire-orientation that are orders of magnitude worse than the epitaxial growth, and (b) several wires per catalyst dot.[12−14] This seriously limits NW's applications, since many high-performance device applications require amorphous insulating substrates.[15,16]

To find a potential solution to overcome the problem, we first need to understand the causes for such large variations. In our view, the variations are related to the behavior of the Au catalyst during a conventional VLS growth[8] on amorphous substrates. First, a pure metal (e.g., Au) catalyst dot often grows multiple NWs rather than one per site and has a NW's diameter that is not determined by the diameter of the original Au dot. One of the reasons is that a pure metal on an amorphous substrate often breaks, during a growth, into multiple smaller catalyst dots of different random sizes (driven by surface energy minimization).[13,14,17,18] However, it has been observed that even without breaking of a catalyst, a single catalyst dot with a thickness-to-width ratio of greater than 0.6 still grows more than one nanowires per dot.[36] Second, the NW's length depends on the incubation time[13,14] and nanowire growth rate.[19,20] On amorphous substrate, the incubation time varies drastically due to random particle size, leading to the difference in NW length. And third, neither the Au catalyst dot nor the underlying amorphous substrate provides a preferred crystal orientation, hence resulting in a random orientation in NWs crystalline planes.

To solve these problems, here we propose and demonstrate a new approach that can grow, on amorphous substrate, straight Si NWs with uniform diameter and length, preferred orientation, and one wire per catalyst site. The key in the new approach, termed "nanopattered host-mediated catalyst" (NHC), is to mix a host material with a metal catalyst rather than to use just the metal catalyst alone. The host material, which is the same as the NW crystal to be grown (e.g., Si in our case), will mediate the formation of the metal catalyst, including metal catalyst crystallization, crystal orientation, and maintaining of single metal catalyst.

Specifically, the process has four key steps (Figure 1): (a) patterning nanosquares of a multilayer of the host material (e.g., Si) and the catalyst (e.g., Au) on an amorphous substrate, (b) melting of the multilayer, (c) solidification that turns each nanosquare into a single Au dot formed in the center and surrounded by a Si shell and crystallizes the Au dot to (111) orientation normal to the substrate surface, and (d) etch away the top part of the Si shell to expose Au dot for growth.

Received: August 2, 2011
Revised: October 3, 2011
Published: October 25, 2011

dx.doi.org/10.1021/nl2026663 | *Nano Lett.* 2011, 11, 5247–5251

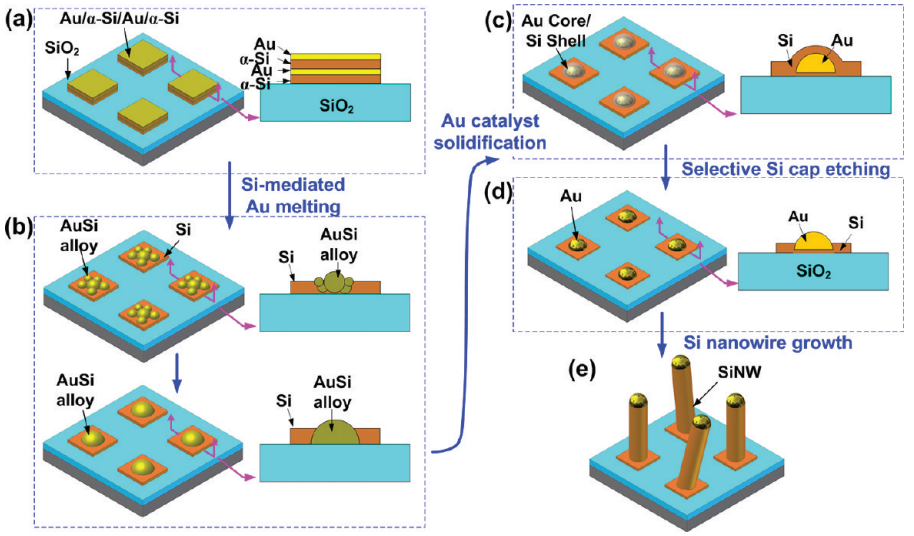

Figure 1. Schematics of fabricating nanopatterned host-medicated catalyst (NHC) for controlled growth of SiNWs. (a) NHC catalysts arrays are initially NIL-patterned squares of Au/α-Si/Au/α-Si thin layers deposited on a SiO_2 substrate. (b) During annealing Au and Si react to form alloy droplets and change the shape. (c) During cooling Au and Si precipitate from the AuSi alloy into one single Au ball surrounded by a Si shell. (d) After wet-etching of Si shell, Au particles are exposed. (e) Grown SiNWs from Au particles.

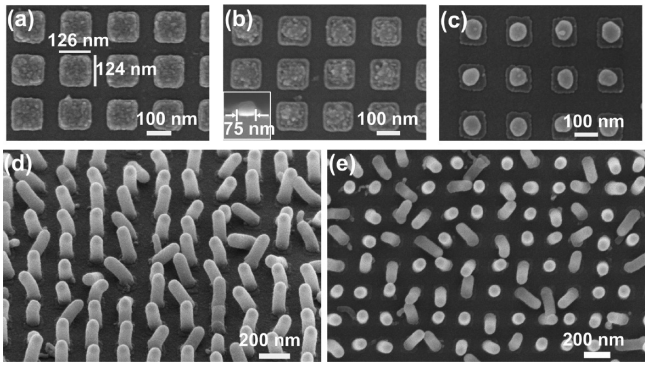

Figure 2. SEM images of NHC catalysts and grown silicon nanowires. (a−c) Top-view image of NHC catalysts at different fabrication steps: (a) as-patterned Au/-Si multilayer nanosquare on the SiO_2 substrate, (b) after annealing (cross-sectional SEM shown as inset), (c) after wet-etching of Si. (d,e) Side-view and top-view images of the SiNWs grown from the NHC.

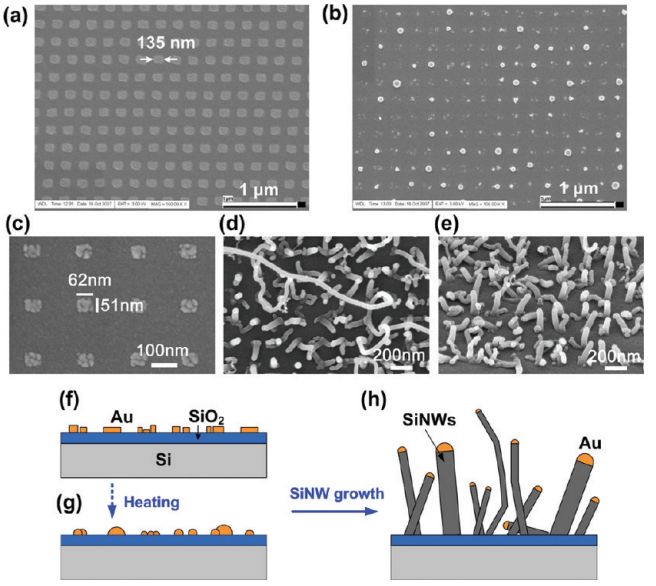

Figure 3. SEM images and schematics of SiNWs grown by conventional single-layer Au catalyst method. (a,b) SEM images of as-patterned and annealed (at 1100 °C) Au dots on SiO_2. (c−e) SEM images of (c) as-patterned 4.3 nm thick Au particles, (d,e) top-view and side-view images of grown nanowires. (f−h) Schematics of nanowire growth (f) as-patterned Au catalysts with gaps, (g) agglomerated Au nanoparticles as heated prior to growth, and (h) nanowires grown from random Au particles.

The formation of a single Au dot is due to full coalescence in mediated meting and subsequent complete separation in cooling. During VLS growth of NWs, the Si shell of host material prevents an Au dot from break-up, provides an additional Si source for the growth and saturates Au with Si. As shown later, this method makes the NWs grow straight and have uniform diameter and length as well as preferred wire-orientation and location.

In one of our NHC experiments, the multilayer nanosquare patterned on a SiO_2 substrate was an array of Au/α-Si/Au/α-Si (nominally 2.9/3.8/3.4/5.7 nm thick layers) multilayer squares of a size 126 × 124 nm^2 (sample A, Figure 2a). They were fabricated by formation of nanosqaure holes in a resist by nanoimprint lithography (NIL),[21,22] e-beam evaporation of Au/Si multilayers onto the imprinted resist, and lift-off. The melting was at 1100 °C for one hour (ramping-up rate ~20 °C/min, cooling-down rate 5−7 °C/min, N_2 ambient, atmospheric pressure). The sample was cooled naturally in air (Figure 2b). A mixture of HF and nitric acid (HF/HNO_3/DI H_2O = 1:2:20) was used to remove the top Si shell (and unintentionally grown SiO_x), exposing the Au nanoparticles for growth (Figure 2c). Finally, the VLS growth of Si NWs using the NHC samples was atmospheric pressure chemical vapor deposition (CVD) ($SiCl_4$/H_2 ratio 8.5%, Ar as carrier and diluting gases) at 1000 °C in a quartz-tube for 5 min.

The SEM inspections of the samples (Figure 2) show that after the annealing one single Au dot was formed at the center of each patterned square (sample A, Figure 2b,c), and consequently one Si-NW was grown from each Au nanodot (Figure 2d,e). On

dx.doi.org/10.1021/nl2026663 |Nano Lett. 2011, 11, 5247–5251

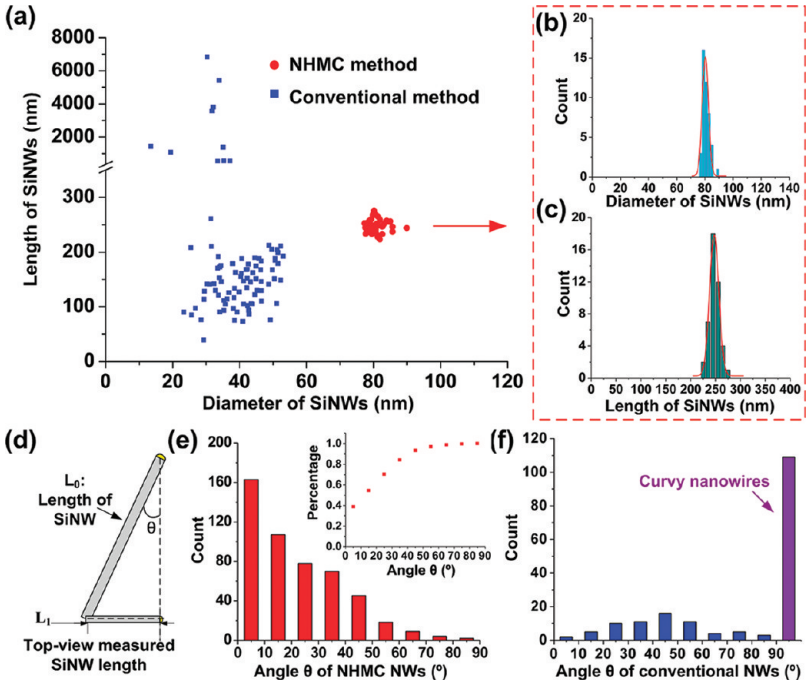

Figure 4. Comparisons of SiNW grown using conventional approach (single-layer Au catalysts) and NHC approach in diameter, length, and orientation. (a) Statistics of lengths and diameters of grown SiNWs. (b,c) Distribution of SiNW lengths and diameters grown using NHC method. (d–f) Statistics of SiNW angles tilted from the substrate surface normal (angle θ): (d) a model for angle calculation, (e) angle distribution of NHC method, and (f) angle distribution of conventional method.

average, the Au nanodots formed have a diameter of 75 nm and a height of 38 nm, and the Si-NWs grown have an average diameter of 81 nm and length of 248 nm. The side-view SEM image (Figure 2d) shows that the Si NWs were straight, mostly vertically aligned, and uniform in length and diameter.

In contrast, the same VLS growth on amorphous substrate using the conventionally prepared pure Au catalyst dots (4.3 nm thick and 62 × 51 nm^2 area, without pregrowth annealing, Figure 3c), had drastically different results: the Si NWs have curvy shapes and a broad distribution of lengths, diameters, and orientations (Figure 3d,e) and an average 2.5 Si NWs per patterned Au catalyst dot. One reason for such different growth results from NHC is the break ups of pure Au pads on the amorphous substrate into several Au dots (Figure 3f–h), which is caused by dewetting of the Au pads[23] with a small thickness-to-width ratio (e.g., 0.08 for our case). However, as pointed earlier, it has been observed that even without breaking of a catalyst, a single catalyst dot with a thickness-to-width ratio of greater than 0.6 still grows more than one nanowires per dot.[36] In fact, to our best knowledge all previous growths of NWs using pure catalyst on an amorphous substrate have led to multiple NWs per catalyst dot and large variation in NW's diameter, length, and orientation. To check the effects of annealing on pure Au on an amorphous substrate, we annealed a pure Au pads (5 nm, 135 nm width, and a thickness-to-width ratio of 0.045) at 1100 °C. We found that after the annealing only part of the pads broke into smaller dots but the rest did not break (SEM, Figure 3a,b). This confirms that Au break up might not be the only reason for the multi-NWs per catalyst site. In comparison, in NHC the thin Au film with even smaller thickness-to-width ratio (0.05) did not break up in the annealing and the growth, but maintained one single Au dot (Figure 2).

The variations of the Si NWs diameters and lengths grown by the NHC growth and the conventional growth were measured using the top-view and cross-sectional SEM images. For the NHC growth, the NW diameter is 81 nm ±3 nm (3.7% deviation), but for the conventional growth it is 39 ± 8 nm (21% deviation), which is about 1 order of magnitude worse. The NW length is 248 nm ±11 nm (4.4% deviation), which is very uniform for the NHC (Figure 4c), but 409 ± 1036 nm (253% deviation) for conventional method, which is about 2 orders of magnitude worse. For the NHC, there is only one NW per catalyst site, but average 2.5 NWs for the conventional growth, which is caused by the break-up of the conventionally patterned Au dots before and during growth (Figure 4a).

The NW alignment uniformity is another critical issue for device integration.[2,24] To characterize the alignment, we measured, using the SEM images, the distribution of zenith angles θ (the angle of SiNWs tilted from the SiO_2 surface normal, Figure 4c), by calculating $\sin\theta = L_1/L_0$ (L_1, the measured in-plane projection length of a nanowire; L_0, the average length, 248 nm). The calculation works well when θ is smaller than 70° with the theoretical error $\Delta\theta = (\Delta L_1)/(L_0 \cos\theta)$ smaller than 3° (assuming $\Delta L_1 = 5$ nm). Using the above equation, we found that most NHC-grown NWs were aligned vertically to SiO_2 substrate within a small angle, that is, 39% of the 496 measured NWs were within 10°, 93% within 50°, and 99% within 70° (Figure 4d,e). For conventionally grown nanowires, only 46% in 173 measured NWs were straight enough for analysis, and their orientation distribution spanned from 0 to 90° without a preferred angle (Figure 4f).

To show that we can control the NW diameter in the NHC growth, we used two other different multilayer Si/Au mixtures to control Au dot diameter: the sample B (124 × 101 nm^2 in area, 2.9/3.8/3.4/5.7 nm of Au/α-Si/Au/α-Si thickness, Figure 5a) and the sample C (48 × 57 nm^2 in area, 2.0/3.7/2.4/4.9 nm in thickness, Figure 5b), leading to the grown Si NWs diameter of 72 and 40 nm, respectively.

dx.doi.org/10.1021/nl2026663 |*Nano Lett.* 2011, 11, 5247–5251

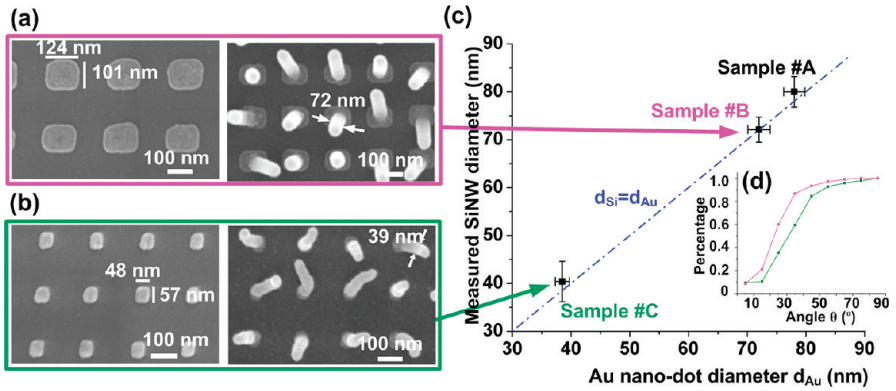

Figure 5. Diameter control of grown SiNWs in NHC growth. (a,b) SEM images of as-patterned catalysts and grown SiNWs of (a) sample B (235 nm pitch, 72 nm diameter SiNWs) and (b) sample C (200 nm pitch, 40 nm diameter SiNWs). (c) The correlation of measured SiNW diameters d_{Si} with diameters of Au hemispheres d_{Au}. (d) The orientation alignment of samples B and C.

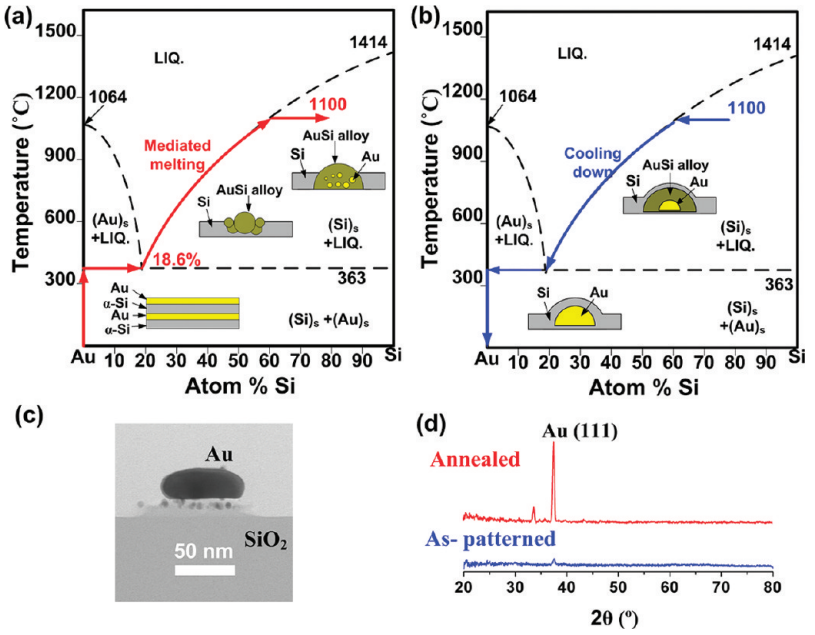

Figure 6. Au catalyst behavior and property in NHC growth. (a,b) Au−Si binary phase diagram with the inserts showing the evolution of NHC catalysts with the red and blue lines indicating the Si concentration change in AuSi system: (a) during mediated melting, (b) during cooling. (c) A STEM cross-sectional image of annealed NHC particle (after wet-etching Si shell). (d) XRD spectra of as-patterned multilayer and annealed (with Si cap etched) samples showing amorphous and (111) crystalline Au phases, respectively.

The measured Si-NW diameter, d_{Si}, was found to be equal to Au catalyst diameter $d_{Au} = [(12/\pi)V_{Au}]^{1/3}$ (which was calculated using deposited Au volume V_{Au} and assuming a hemispherical particle shape) within a 2 nm error (Figure 5c). By controlling the NIL pillar size and Au thickness, we have tuned the Si NW diameter from ~40 to ~80 nm. We believe the tuning range can be wider than what we have achieved, for example, down to sub-10 nm regimes.

The NHC samples B and C have average lengths of ~225 and ~165 nm, respectively. Si NWs on sample B (105 wires measured) have 9% aligned within 10°, 60% within 30°, 93% within 50°, and 99% within 70° from the substrate surface normal, while the sample C (96 NWs measured) has 9, 35, 84, and 96% respectively (Figure 5d). Compared with the conventional growth, the orientation alignment of all NHC samples (A, B, and C) was much better; for example, sample A has 20 times more wires aligned within 10° than conventional sample (<2%).

In our approach, NIL was used not only for its patterning accuracy, but also for its high-throughput, large-area, and high-density patterning abilities. The spatial densities of our NWs were 25 wires/μm^2 for 200 nm period NIL molds, which is much higher than using Au colloids (0.1−1.8 wires/μm^2)[10] and photolithography-patterned Au microparticles (0.02 wires/μm^2).[25] The NW density can be further increased by reducing the patterning period.

The reason for the NHC growth on an amorphous substrate having straight silicon NW array with uniform length and diameter, preferred orientation, and predetermined location is that the host material in the NHC (a) ensures one single metal catalyst dot per growth site, (b) prevents the catalyst dot break-up during the growth, (c) provides an additional material source for the NW growth, and (d) crystallizes both the metal catalyst and the Si seeding layer to control Si NW orientation.

In the pregrowth annealing, the Au multilayers melt into small Au dots first and then coalesce into one single large Au dot surrounded

dx.doi.org/10.1021/nl2026663 |*Nano Lett.* 2011, 11, 5247–5251

by Si. Such a process is clearly energetically favored by the Au−Si phase diagram (Figure 6a,b). At 363 °C,[26] Au−Si alloy melt starts melting. As the annealing temperature rises, the melt will increase and eventually spread to the entire nanosquare. Also, the completely molten AuSi alloy will reshape from the nanosquare to a hemisphere (Figure 6a). This is because AuSi alloy has a large volume (~3 times larger than Au at 1100 °C with 65% Si[26]), small surface energy (~30% smaller than Au),[27] and a good wetting ability on SiO_2.[28] Upon cooling (blue arrows, Figure 6b), the Si and Au separate from each completely due to their negligibly small mutual solubilities (<2×10^{-4} % Au in Si[29] and ~0.1% Si in Au)[37] with a Si in a form of a shell surrounding Au due to the smaller surface energy of Si than Au.[27] This fact is clearly seen in our scanning transmission electron microscopy (STEM) image (Figure 5c), show one single Au ball forms on a Si base (after Si top shell etched).

The X-ray diffraction (XRD) spectra (Figure 6d) show that the Au dot in NHC is crystallized with (111) direction normal to substrate surface during the pregrowth annealing. It has been known that annealing of face-centered cubic (fcc) metal (such as Au) or diamond material (such as Si) leads to the preferred crystallization of (111) plane parallel to substrates,[23,30−32] because (111) planes are most densely packed and thus the surface/interface energies are minimized.[23] It is expected that the pregrowth annealing will also crystallize the thin Si base layer to (111). Such possibility has been demonstrated in both microscale[33,34] and nanoscale.[34,35] However, in our case the (111) Si texture is not clear from XRD, probably because the layer is too thin (<13 nm) and embedded with some <5 nm Au particles precipitated from annealing (Figure 6c). As a result, the (111) crystal Au nanoparticles, together with the thin Si layer (expected (111) crystallized after the annealing with Au), seed the growth of Si NWs into ⟨111⟩ orientation and vertical to the substrate.

Moreover, the Si shell could provide the Si source during the early stage of NW growth for AuSi alloy saturation and thus eliminate the difference in NW incubation time,[13,14] further unifying the NW growth.

In summary, we have proposed and demonstrated a new approach, namely NHC growth, to grow Si NWs, on amorphous substrates, uniformly (<5% deviation in diameter and length) and aligned vertically (70% within 30°) with Si NWs in ⟨111⟩ orientations. The results are far better than conventional growth using pure Au catalysts (21% deviation in diameter, 253% deviation in length, random orientation, and curvy shape). The NHC growth also offers the highest NW density (25 wires/μm^2 or even larger). The NHC can be extended to grow other semiconductor nanowires (Ge, SiGe, ZnO, III−V materials, II−IV materials, and so forth), and applicable to many different substrates and broad electrical, optical, and bio/chemical applications.

AUTHOR INFORMATION

Corresponding Author

*E-mail: chou@princeton.edu.

ACKNOWLEDGMENT

The authors thank Maiofang Chi and Ray Twesten from Gatan Inc. for help on the compositional analysis and appreciate the helpful discussions with Professor Sigurd Wagner, Dr. Zengli Fu, Dr. Xiaogan Liang, Dr. Keith. J. Mortan, Dr. Keith H. Chang, and Dr. Yu Yao from Princeton University. The work was partially supported by a Defense Advanced Research Projects Agency (DARPA) MTO grant (a subcontract through Stanford University) and the National Science Foundation through the grants to SYC and MRSEC program through the Princeton Center for Complex Materials (DMR-0819860).

REFERENCES

(1) Cui, Y.; Lieber, C. M. *Science* **2001**, *291*, 851–853.
(2) Thelander, C.; Agarwal, P.; Brongersma, S.; Eymery, J.; Feiner, L. F.; Forchel, A.; Scheffler, M.; Riess, W.; Ohlsson, B. J.; Gosele, U.; Samuelson, L. *Mater. Today* **2006**, *9*, 28–35.
(3) Huang, M. H.; Mao, S.; Feick, H.; Yan, H. Q.; Wu, Y. Y.; Kind, H.; Weber, E.; Russo, R.; Yang, P. D. *Science* **2001**, *292*, 1897–1899.
(4) Law, M.; Greene, L. E.; Johnson, J. C.; Saykally, R.; Yang, P. D. *Nat. Mater.* **2005**, *4*, 455–459.
(5) Sun, X. W.; Wang, J. X. *Nano Lett.* **2008**, *8*, 1884–1889.
(6) Patolsky, F.; Zheng, G. F.; Hayden, O.; Lakadamyali, M.; Zhuang, X. W.; Lieber, C. M. *Proc. Natl. Acad. Sci. U.S.A.* **2004**, *101*, 14017–14022.
(7) Xia, Y. N.; Yang, P. D.; Sun, Y. G.; Wu, Y. Y.; Mayers, B.; Gates, B.; Yin, Y. D.; Kim, F.; Yan, Y. Q. *Adv. Mater.* **2003**, *15*, 353–389.
(8) Wagner, R. S.; Ellis, W. C. *Appl. Phys. Lett.* **1964**, *4*, 89–90.
(9) Westwater, J.; Gosain, D. P.; Tomiya, S.; Usui, S.; Ruda, H. *J. Vac. Sci. Technol., B* **1997**, *15*, 554–557.
(10) Hochbaum, A. I.; Fan, R.; He, R. R.; Yang, P. D. *Nano Lett.* **2005**, *5*, 457–460.
(11) Schmidt, V.; Senz, S.; Gosele, U. *Nano Lett.* **2005**, *5*, 931–935.
(12) Cui, Y.; Lauhon, L. J.; Gudiksen, M. S.; Wang, J. F.; Lieber, C. M. *Appl. Phys. Lett.* **2001**, *78*, 2214–2216.
(13) Kawashima, T.; Mizutani, T.; Masuda, H.; Saitoh, T.; Fujii, M. *J. Phys. Chem. C* **2008**, *112*, 17121–17126.
(14) Hofmann, S.; Sharma, R.; Wirth, C. T.; Cervantes-Sodi, F.; Ducati, C.; Kasama, T.; Dunin-Borkowski, R. E.; Drucker, J.; Bennett, P.; Robertson, J. *Nat. Mater.* **2008**, *7*, 372–375.
(15) Shahidi, G. G. *IBM J. Res. Dev.* **2002**, *46*, 121–131.
(16) Liu, A. S.; Jones, R.; Liao, L.; Samara-Rubio, D.; Rubin, D.; Cohen, O.; Nicolaescu, R.; Paniccia, M. *Nature* **2004**, *427*, 615–618.
(17) Colli, A.; Fasoli, A.; Beecher, P.; Servati, P.; Pisana, S.; Fu, Y.; Flewitt, A. J.; Milne, W. I.; Robertson, J.; Ducati, C.; De Franceschi, S.; Hofmann, S.; Ferrari, A. C. *J. Appl. Phys.* **2007**, *102*, 034302.
(18) Jiran, E.; Thompson, C. V. *J. Electron. Mater.* **1990**, *19*, 1153–1160.
(19) Givargizov, E. I. *J. Cryst. Growth* **1975**, *31*, 20–30.
(20) Kikkawa, J.; Ohno, Y.; Takeda, S. *Appl. Phys. Lett.* **2005**, *86*, 123109.
(21) Chou, S. Y.; Krauss, P. R.; Renstrom, P. J. *Science* **1996**, *272*, 85–87.
(22) Chou, S. Y.; Krauss, P. R.; Zhang, W.; Guo, L. J.; Zhuang, L. *J. Vac. Sci. Technol., B* **1997**, *15*, 2897–2904.
(23) Thompson, C. V. *Annu. Rev. Mater. Sci.* **1990**, *20*, 245–268.
(24) Fan, H. J.; Werner, P.; Zacharias, M. *Small* **2006**, *2*, 700–717.
(25) Kayes, B. M.; Filler, M. A.; Putnam, M. C.; Kelzenberg, M. D.; Lewis, N. S.; Atwater, H. A. *Appl. Phys. Lett.* **2007**, *91*, 103110.
(26) Okamoto, H.; Massalski, T. B. *J. Phase Equilib.* **1983**, *4*, 190–198.
(27) Naidich, Y. V.; Perevertailo, V. M.; Obushchak, L. P. *Powder Metall. Met. Ceram.* **1975**, *14*, 403–404.
(28) Tu, K. N.; Libertini, S. H. *J. Appl. Phys.* **1977**, *48*, 420–421.
(29) Collins, C. B.; Carlson, R. O.; Gallagher, C. J. *Phys. Rev.* **1957**, *105*, 1168–1173.
(30) Givargizov, E. I. *Heterog. Chem. Rev.* **1995**, *2*, 69–78.
(31) Thompson, C. V.; Carel, R. *Mater. Sci. Eng., B* **1995**, *32*, 211–219.
(32) Giermann, A. L.; Thompson, C. V. *Appl. Phys. Lett.* **2005**, *86*, 121903.
(33) Ishiwata., K; Oka, T.; Akiyama, K. *Jpn. J. Appl. Phys.* **1967**, *6*, 1170–1175.
(34) Mori, H. *Jpn. J. Appl. Phys.* **1981**, *20*, L905–L908.
(35) Chandra, A.; Clemens, B. M. *J. Appl. Phys.* **2004**, *96*, 6776–6781.
(36) Javey, A; Dai, H. *J. Am. Chem. Soc.* **2005**, *127*, 11942–11943.
(37) Johnson, D. N.; Biagtan, E. C.; Johnson, A. A. *Scr. Metall.* **1987**, *21*, 1689–1692.